# A Vacuum Ultraviolet Photoionization Mass Spectrometric Study of Ethylene Oxide in the Photon Energy Region of 10−40 eV

**Fuyi Liu, Fei Qi, Hui Gao, Liusi Sheng, and Yunwu Zhang**

*National Synchrotron Radiation Laboratory, University of Science and Technology of China, Hefei, Anhui 230026, People's Republic of China*

**Shuqin Yu**

*Department of Chemical Physics, University of Science and Technology of China, Hefei, Anhui 230026, People's Republic of China*

**Kai-Chung Lau and Wai-Kee Li***

*Department of Chemistry, The Chinese University of Hong Kong, Shatin, N.T., Hong Kong*

*Received: December 4, 1998; In Final Form: February 11, 1999*

The photoionization and dissociative photoionizations of ethylene oxide have been studied both experimentally and theoretically. In experiments, photoionization efficiency spectra for ions $C_2H_4O^+$, $C_2H_3O^+$, $C_2H_2O^+$, $C_2HO^+$, $CH_3O^+$, $CH_2O^+$, $CHO^+$, $C_2H_4^+$, $C_2H_3^+$, $C_2H_2^+$, $C_2H^+$, $CH_4^+$, $CH_3^+$, $CH_2^+$, $CH^+$, and $C^+$ have been obtained. In addition, the energetics of the dissociative photoionizations have been examined by ab initio Gaussian-2 calculations. The computational results are useful in establishing the dissociation channels near the ionization thresholds. The dissociation channels established may be broadly divided into two types: simple bond cleavage reactions and those involving transition structures and activation energies.

## Introduction

Ethylene oxide is an important compound with two interesting structural features. The first one is the strong ring strain. The second one is that, with an oxygen atom in the ring, there are polar covalent bonds in the molecules. Additionally, it has been established that the 1,2-epoxy functional group plays an important role in the biological activities of a large number of natural products.[1] Hence, a better understanding of the energetics for epoxy compounds is clearly desirable. In this work, we report a quantitative study on the photoionization and dissociative photoionizations of ethylene oxide.

Previously, Gallegos and Kiser[2] used electron impact (EI) to initiate the ionization and dissociation processes of ethylene oxide with time-of-flight mass spectrometry (TOF-MS). Subsequently, Krassig and co-workers[3] studied the analogous processes using a vaccum ultraviolet (VUV) discharge lamp. Both of these reports include the appearance energies (AEs) of the principal fragment ions in the mass spectra of ethylene oxide and suggest possible ionization/dissociation channels. Moreover, the ionization energy (IE) of ethylene oxide has been measured by various groups using EI,[2,4,5] photoelectron spectroscopy,[6−10] and photoionization[3,8,11,12] (PI) techniques. However, the data these researches reported are rather scattered, due to the very low ion production efficiency near the ionization threshold. Also, hot band effects, ion/molecule reactions, etc., often cause difficulties in the accurate determination of the AEs. Here, the experiments were carried out under supersonic conditions, thereby overcoming the effects of the aforementioned secondary processes. The light source we employed was high intensity synchrotron radiation, which is particularly suitable for the photoionization processes of a molecule. Also, the wavelength was scanned continuously and hence the thresholds can be measured accurately.

In the present work, we report the photoionization efficiency (PIE) curves of all ions resulting from the dissociative photoionizations of ethylene oxide in the photon energy region of 10−40 eV. From these PIE data, we can derive the energetics of the dissociations. Combining these results with high level ab initio calculations, the various dissociation channels of ethylene oxide can then be established.

## Experimental and Theoretical Methods

The experimental and computational techniques employed in this work have been used to study the dissociations of ammonia,[13] vinyl chloride,[14] dichlorodifluoromethane,[15] and carbon tetrachloride.[16] A description of these techniques is given below.

**Experimental Method.** The experimental setup has been described in previous publications,[13−16] and it is briefly outlined here. Synchrotron radiation from the 800 MeV electron storage ring (National Synchrotron Radiation Laboratory, Hefei, Anhui, China) is monochromized by using a 1 m Seya-Namioka monochromator equipped with two gratings (2400 and 1200 lines $mm^{-1}$) covering the wavelength range from 30 to 300 nm. The absolute wavelength of monochromator was calibrated with the known IEs and autoionization peaks of the inert gases He, Ne, and Ar. The wavelength resolution is about 0.1 nm with 150 $\mu$m entrance and exit slits. The photon flux was monitored by a sodium salicylate coated glass window with a photomultiplier tube behind the ionization chamber. The PIE curves were normalized by the photon flux. A LiF cutoff filter (1 mm thickness) was used to eliminate higher order radiation of the dispersed light in the wavelength region longer than the LiF cutoff wavelength (105 nm).

A TOF-MS was employed for the VUV photoionization/fragmentation studies. Photoions produced by the VUV light

10.1021/jp984626b CCC: $18.00 
Published on Web 05/11/1999

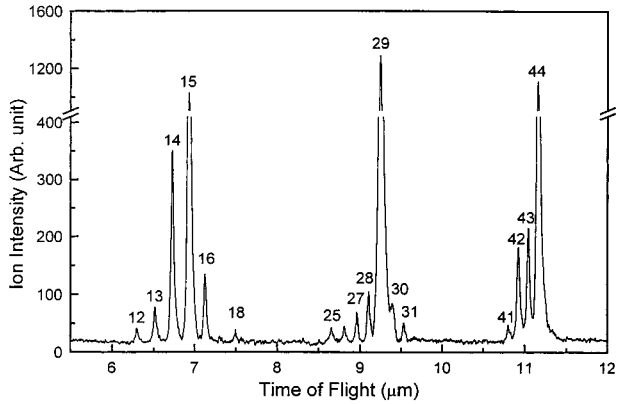


**Figure 1.** Photoionization TOF-mass spectrum of ethylene oxide at the wavelength of 30 nm.

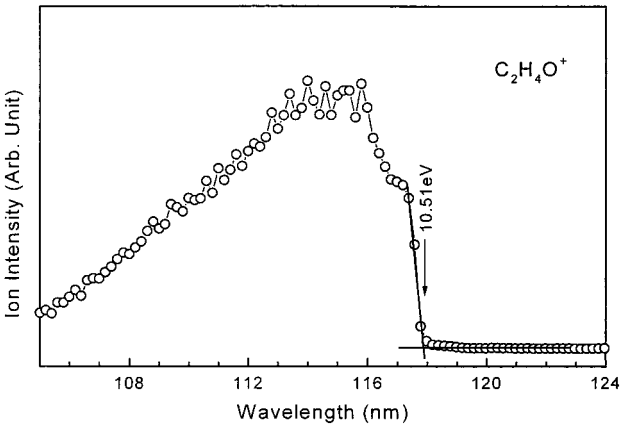


**Figure 2.** Photoionization yield curve of parent ion $C_2H_4O^+$.

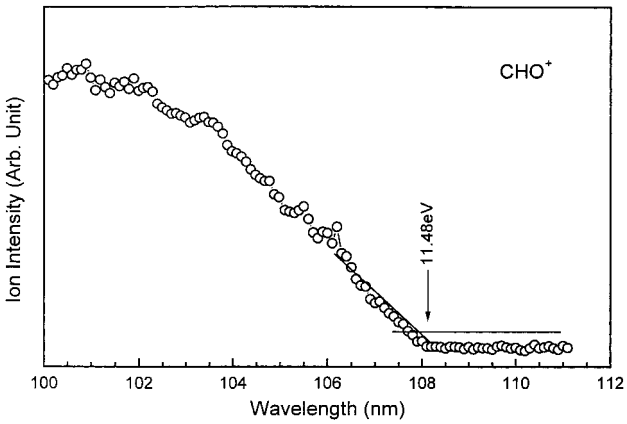


**Figure 3.** Photoionization efficiency curve of $CHO^+$ from ethylene oxide.

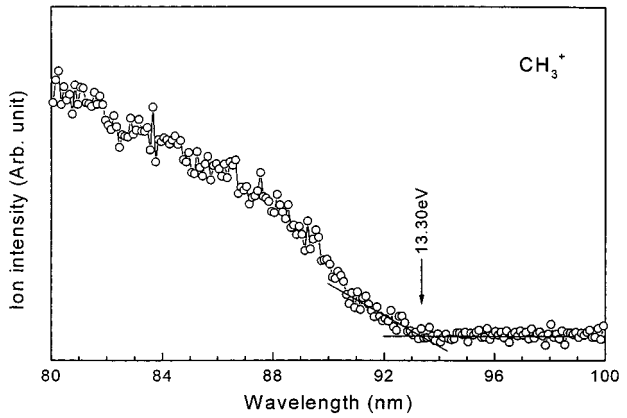


**Figure 4.** Photoionization efficiency curve of $CH_3^+$ from ethylene oxide.

were drawn out of the photoionization region, by a pulse extraction field triggered with a pulse signal generator and detected by a microchannel plate detector. The photoion signal was discriminated and used to stop a time-to-amplitude converter (TAC) which was started with the pulse signal generator. The output of the TAC was sorted in a multichannel analyzer. A mass spectrum was obtained as the photoion number vs the flight time of the ions. The TOF tube is 0.4 m long and its mass resolution is larger than 200. A specified ion can be selected with the TAC combined with a single-channel analyzer. The ion signal intensity was controlled so as to avoid the parasitic effect in using the TAC for the TOF measurements. The PIE curve was obtained as the wavelength was scanned with a wavelength step of 0.1 nm. The PIE curves of some daughter ions of weak signals were obtained by recording a series of TOF mass spectra at different wavelengths with a wavelength increment of 1 nm. The AEs of these ions were estimated by taking the wavelength at which the ion disappears.

The vapor of ethylene oxide sample (purity 99%) was introduced by supersonic expansion through a continuous beam nozzle (70 $\mu$m diameter) from the molecular beam chamber into the ionization chamber through a 1 mm skimmer. In this experiment, He (purity 99.999%) was used as the carrier gas and the stagnation pressure was about 0.1 MPa. The pressure of the ionization chamber was about $8 \times 10^{-5}$ Pa when the molecule beam was introduced. No cluster was observed under this condition, so no fragment ions were considered to originate from cluster dissociation.

**Computational Method.** The Gaussian-2 (G2) theoretical procedure[17] is an approximation for the QCISD(T)/6-311+G-(3df,2p) energy. It involves single-point calculations at the MP4/6-311G(d,p), QCISD(T)/6-311G(d,p), MP4/6-311+G(d,p), MP4/6-311G(2df,p), and MP2/6-311+G(3df,2p) levels, all carried out with the structures optimized at the MP2(Full)/6-31G(d) level. The HF/6-31G(d) harmonic frequencies, scaled by 0.8929, are used for correction of zero-point vibrational energies. A small semiempirical correction is also applied to account for the high level correlation effect. We have applied this method to a variety of chemical systems.[14−16] The agreement between G2 and experimental results is usually well within ± 0.15 eV. All the computations involved in this work were carried out on SGI R10000 workstation and SGI Origin 2000 high performance server using the Gaussian 94 suite of programs.[18]

## Results and Discussion

**Experimental Measurements.** The TOF mass spectrum of ethylene oxide at wavelength 30 nm is shown in Figure 1. As can be seen from the figure, in addition to the parent ion $C_2H_4O^+$ and the fragment ions $C_2H_3O^+$, $C_2H_2O^+$, $CHO^+$, $CH_4^+$, and $CH_3^+$, other smaller fragment ions can also be identified. The mass peaks at $m/e = 18$ and 17 have been ignored because they come from the photoionization of background water molecule in the ionization chamber.

The PIE curves of the parent ion $C_2H_4O^+$ and of the higher intensity fragment ions $C_2H_3O^+$, $C_2H_2O^+$, $CHO^+$, $C_2H_4^+$, $C_2H_3^+$, $CH_4^+$, $CH_3^+$, and $CH_2^+$ from ethylene oxide, were obtained by scanning continuously the wavelength of the grating. Figures 2−4 show, respectively, the PIE spectra of the parent ion $C_2H_4O^+$ and of the fragment ions $CHO^+$ and $CH_3^+$. The AE in each PIE curve was determined by the linear extrapolation method.[13,14,19] It should be pointed out that we ignored the

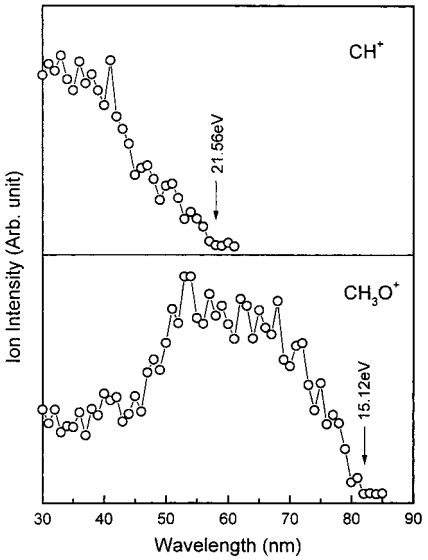


**Figure 5.** Photoionization efficiency curves of $CH^+$ and $CH_3O^+$ from ethylene oxide.

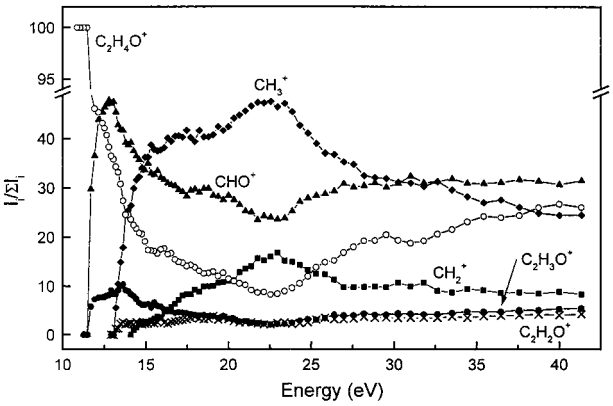


**Figure 6.** Relative intensity of major ions from ethylene oxide. The intensity sum of all major ions is set to be 100.

**TABLE 1: Appearance Energies (eV) Measured in the Dissociative Photoionizations of Ethylene Oxide**

| *m/e* | ion | this work | PI[a] | EI[b] |
|---|---|---|---|---|
| 44 | $C_2H_4O^{+c}$ | 10.51 ± 0.02 | 10.56 | 10.65 |
| 43 | $C_2H_3O^{+d}$ | 11.80 ± 0.02 | 11.62 | 12.1 |
| 42 | $C_2H_2O^+$ | 13.62 ± 0.03 | 13.07 | 14.0 |
| 41 | $C_2HO^+$ | 17.46 ± 0.15 | | |
| 31 | $CH_3O^+$ | 15.12 ± 0.10 | | |
| 30 | $CH_2O^+$ | 14.25 ± 0.10 | | |
| 29 | $CHO^+$ | 11.48 ± 0.02 | 11.54 | 12.2 |
| 28 | $C_2H_4^+$ | 14.18 ± 0.03 | | |
| 28 | $CO^+$ | | | 12.6 |
| 27 | $C_2H_3^+$ | 12.78 ± 0.02 | 12.92 | 14.3 |
| 26 | $C_2H_2^+$ | 11.81 ± 0.06 | | 15.7 |
| 25 | $C_2H^+$ | 27.55 ± 0.30 | | 24.0 |
| 16 | $CH_4^+$ | 11.50 ± 0.02 | 11.79 | 12.3 |
| 15 | $CH_3^+$ | 13.30 ± 0.03 | 13.06 | 14.3 |
| 14 | $CH_2^+$ | 13.65 ± 0.03 | 14.66 | 16.5 |
| 13 | $CH^+$ | 21.56 ± 0.20 | | 22.8 |
| 12 | $C^+$ | 25.83 ± 0.30 | | |

[a] Data obtained using photoionization techniques, taken from ref 3. [b] Data obtained using electron impact, taken from ref 2. [c] Other reported values for this ion include 10.15 (ref 5), 10.57 (refs 4, 6, 10, and 12), 10.4 (ref 9), 10.56 (ref 8), 10.558 (ref 8), 10.568 (ref 7), 10.565 eV (ref 11). [d] Another reported value for this ion is 11.53 eV (ref 4).

thermal energy distribution of the parent molecule in our data treatment, considering the present nozzle expansion condition described above. In addition, no correction was made for possible kinetic shifts in determining the AEs. Similar data analysis have been carried out by other researchers, and it appears to be useful for studying ion fragmentation processes.[20−22]

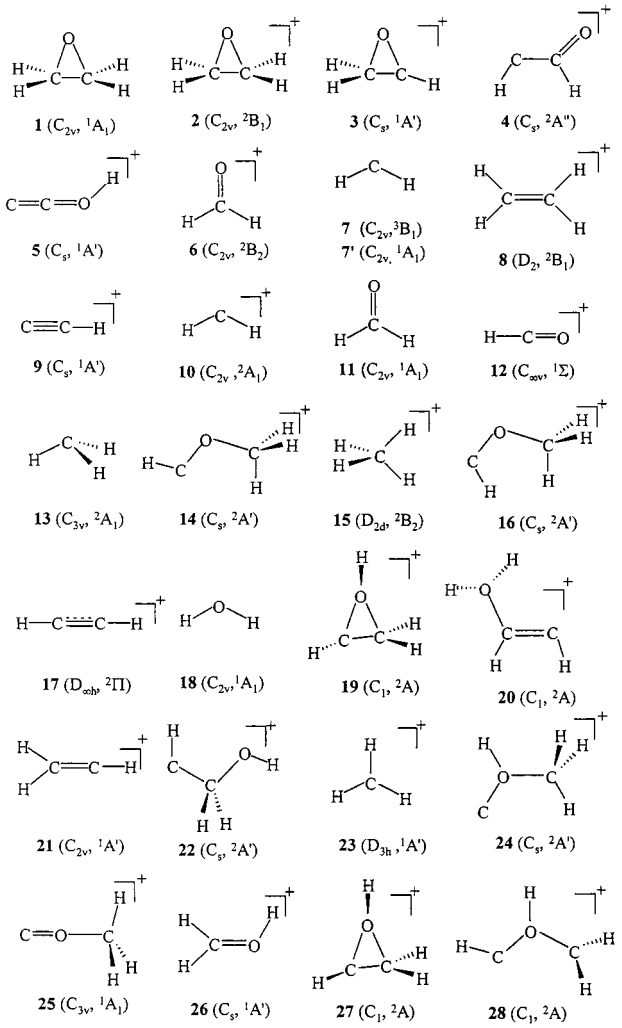


**Figure 7.** Structural formulas of the various polyatomic species (with three or more atoms) involved in this work, along with their symmetry point groups and electronic states.

Since the signals of the other fragments are quite weak, continuous wavelength scanning of these fragment channels was not pursued. Instead, we took the TOF mass spectra with 1 nm intervals from 30 to 120 nm and constructed PIE curves based on these mass spectra. The AEs of these ion fragments were determined as the photon energy at which the ion disappears. Figure 5 shows the PIE curves of the fragment ions $CH^+$ and $CH_3O^+$. The AEs of these fragment ions were determined for the first time by this method.

Shown in Figure 6 is the relative ion abundance as a function of photon energy for the parent ion and several major fragment ions $C_2H_3O^+$, $C_2H_2O^+$, $CHO^+$, $CH_3^+$, and $CH_2^+$ from the dissociative photoionizations of ethylene oxide. The ion intensities are normalized so that their intensity sum is 100 at any wavelength. Figure 6 shows that, at low photon energy, the parent ion predominates. As the photon energy is increased, the fragment ion $CHO^+$ appears first, then other ion fragments come into view successively. Approximately, the abundance of each of these ions passes through a maximum and then decreases to a nearly constant value at high energy except those of $C_2H_4O^+$ and $CHO^+$. The abundance values of $C_2H_4O^+$ and $CHO^+$ start to increase at the photon energy of about 22.5 eV. It is interesting that this photon energy is also the knee points of

**TABLE 2: The G2 Energies ($E_0$(G2)) of Various Species Involved in the Dissociation of Ethylene Oxide and Its Cation**

| species | $E_0$(G2)/hartree | species | $E_0$(G2)/hartree |
|---|---|---|---|
| $C_2H_4O$ (**1**) | −153.532 89 | $CH_3OC^+$ (**25**) | −152.596 83 |
| $C_2H_4O^+$ (**2**) | −153.142 03 | $CH_3O^+$ (**26**) | −114.607 76 |
| $C_2H_3O^+$ (**3**) | −152.592 68 | *cis*-c-$CHOHCH_2^+$ (**27**) | −153.138 76 |
| $C_2H_2O^+$ (**4**) | −151.855 47 | $CHOHCH_2^+$ (**28**) | −153.042 61 |
| $C_2HO^+$ (**5**) | −151.223 55 | H[a] | −0.500 00 |
| $CH_2O^+$ (**6**) | −113.936 26 | O[a] | −74.982 03 |
| $CH_2$ (**7**) | −39.069 00 | $C^+$[a] | −37.373 45 |
| $CH_2$ (**7′**) | −39.058 40 | CO[a] | −113.177 49 |
| $C_2H_4^+$ (**8**) | −78.026 31 | $H_2$[a] | −1.166 36 |
| $C_2H^+$ (**9**) | −76.037 33 | OH[a] | −75.643 91 |
| $CH_2^+$ (**10**) | −38.690 06 | CH ($^4\Sigma$) | −38.381 71 |
| $CH_2O$[a] (**11**) | −114.338 92 | $CH^+$ ($^1\Sigma$) | −38.024 47 |
| $HCO^+$ (**12**) | −113.401 11 | transition structures[b] | |
| $CH_3$[a] (**13**) | −39.745 09 | TSa | −153.106 87 |
| *trans*-$HCOCH_3^+$ (**14**) | −153.164 41 | TSb | −153.137 40 |
| $CH_4^+$ (**15**) | −39.940 45 | TSd | −153.087 49 |
| *cis*-$HCOCH_3^+$ (**16**) | −153.159 76 | TSe | −153.098 20 |
| $C_2H_2^+$ (**17**) | −76.765 99 | TSf | −153.097 76 |
| $H_2O$[a] (**18**) | −76.332 05 | TSg | −153.060 15 |
| *trans*-c-$CHOHCH_2^+$ (**19**) | −153.139 81 | TSh | −153.036 35 |
| $CHCHOH_2^+$ (**20**) | −153.148 70 | TSi | −153.049 03 |
| $C_2H_3^+$ (**21**) | −77.423 49 | TSj | −153.134 67 |
| $CHCH_2OH^+$ (**22**) | −153.105 63 | TSk | −153.027 45 |
| $CH_3^+$ (**23**) | −39.385 59 | TSl | −152.971 64 |
| $CH_3OHC^+$ (**24**) | −153.080 38 | | |

[a] Values taken from ref 17. [b] The transition structures TSa to TSl are defined in Figures 8-13.

the abundance of $C_2H_3^+$ and $CH_2^+$. The reason of this phenomenon is not clear at present. At the photon energy of above about 14 eV, the abundance of $CHO^+$ and $CH_3^+$ are above those of all the other ions. Therefore, the channels of forming $CHO^+$ and $CH_3^+$ (transannular cleavage with hydrogen transfer) are the principal dissociative photoionization channels of ethylene oxide. Since the relative ion abundance graph is constructed from a series of TOF mass spectra with a relatively large wavelength interval (1 nm), some fine features have been lost.

All the AEs obtained from the PIE curves are listed in Table 1, along with the values measured by other researchers. The error ranges are also listed. These errors reflect either the bandwidth of our monochromator or the wavelength interval of the data points for performing the measurements. The AEs of the fragment ions $C_2HO^+$, $CH_3O^+$, $CH_2O^+$, $C_2H_4^+$, $C_2H_2^+$, $C_2H^+$, $CH^+$, and $C^+$ from the dissociative photoionizations of ethylene oxide have been obtained previously by using synchrotron radiation photoionization, while the AE values of $C_2HO^+$, $CH_3O^+$, and $C^+$ are reported for the first time. The ion AEs we reported here are very close to those obtained by using photoionization method,[3] but lower than those obtained by the EI ionization method.[2] This is understandable since it is known that the EI ionization method often overestimates AEs of both parent and fragment ions. The IE of ethylene oxide we have measured is a bit lower than all the reported values in the literature except those of refs 5 and 9. It should be mentioned that, in measuring the AEs of $C_2H_4O^+$, $C_2H_3O^+$, $CHO^+$, and $CH_4^+$, a LiF filter was used to eliminate the effect of higher order radiation from the grating. For the AE measurements of $C_2H_2O^+$, $C_2H_4^+$, $C_2H_3^+$, $C_2H_2^+$, $CH_3^+$, and $CH_2^+$, no filter was used. According to past experience, the effect of the second-order radiation from the grating of 2400 lines $mm^{-1}$ is negligible.[13,14] Because of the adoption of the continuously wavelength scanning technique and the usage of the LiF filter to eliminate the higher order radiation, our photoionization onset in the PIE curve of parent ion $C_2H_4O^+$ in Figure 2 appears quite sharp and clear. In addition, our experiments were carried out under supersonic cooling conditions, thereby overcoming the hot band effect and other influences on the accurate determination of the AEs. Also, the light source employed was high-intensity synchrotron radiation. We therefore believe that the IE of ethylene oxide we have obtained is more accurate than those of the previous measurements.

**Computational Results.** The structural formulas of the polyatomic species (with three or more atoms) involved in this work, along with their symmetry point groups and electronic states, are displayed in Figure 7. The calculated G2 energies ($E_0$(G2)) of various species involved in the dissociations of ethylene oxide (**1**) and its cation (**2**) are summarized in Table 2. With the aid of these results, we have established the dissociation channels of ethylene oxide cation.

With the $E_0$(G2) values of **1** and **2**, the IE of ethylene oxide is calculated to be 10.64 eV. Considering that the error range for G2 results is ± 0.15 eV, this calculated value is in agreement with the experimental result, 10.51 ± 0.02 eV.

**Simple Bond Cleavage Reactions.** Dissociations of the ethylene oxide cation (**2**), which involve only the cleavage of bond(s), are summarized in this section.

$$C_2H_4O^+ (\mathbf{2}) \xrightarrow{\Delta E_1} C_2H_3O^+ (\mathbf{3}) + H \qquad (1)$$

$$\Delta E_1 = AE(C_2H_3O^+) - IE(C_2H_4O) = 1.29 \pm 0.02 \text{ eV}$$

It is noted that we did locate a transition structure (TS) for this dissociation reaction. In this TS, the length of the C−H "bond" that is being broken is about 1.690 Å. However, the G2 energy of this TS is 1.32 eV above that of **2**, while that of the dissociated products (calculated from results listed in Table 2) is 1.34 eV. In other words, this TS has an energy that is *lower* than that of the products. Hence, it is not certain that if this TS exists or not. But, even if it does, its energy should be very close to that of the products.

$$C_2H_4O^+ (\mathbf{2}) \xrightarrow{\Delta E_2} C_2H_2O^+ (\mathbf{4}) + H_2 \qquad (2)$$

$$\Delta E_2 = AE(C_2H_2O^+) - IE(C_2H_4O) = 3.11 \pm 0.03 \text{ eV}$$

$$C_2H_4O^+ (\mathbf{2}) \xrightarrow{\Delta E_3} C_2HO^+ (\mathbf{5}) + H_2 + H \quad (3)$$

$$\Delta E_3 = AE(C_2HO^+) - IE(C_2H_4O) = 6.95 \pm 0.15 \text{ eV}$$

$$C_2H_4O^+ (\mathbf{2}) \xrightarrow{\Delta E_4} CH_2O^+ (\mathbf{6}) + CH_2 (\mathbf{7}) \quad (4)$$

$$\Delta E_4 = AE(CH_2O^+) - IE(C_2H_4O) = 3.74 \pm 0.10 \text{ eV}$$

$$C_2H_4O^+ (\mathbf{2}) \xrightarrow{\Delta E_5} C_2H_4^+ (\mathbf{8}) + O \quad (5)$$

$$\Delta E_5 = AE(C_2H_4^+) - IE(C_2H_4O) = 3.67 \pm 0.03 \text{ eV}$$

$$C_2H_4O^+ (\mathbf{2}) \xrightarrow{\Delta E_6} C_2H^+ (\mathbf{9}) + 3H + O \quad (6)$$

$$\Delta E_6 = AE(C_2H^+) - IE(C_2H_4O) = 17.04 \pm 0.30 \text{ eV}$$

$$C_2H_4O^+ (\mathbf{2}) \xrightarrow{\Delta E_7} CH_2^+ (\mathbf{10}) + CH_2O (\mathbf{11}) \quad (7)$$

$$\text{or } CH_2^+ (\mathbf{10}) + CO + H_2$$

$$\Delta E_7 = AE(CH_2^+) - IE(C_2H_4O) = 3.14 \pm 0.03 \text{ eV}$$

$$C_2H_4O^+ (\mathbf{2}) \xrightarrow{\Delta E_8} CH^+ (^1\Sigma) + CH_2 (\mathbf{7}) + OH \quad (8)$$

$$\Delta E_8 = AE(CH^+) - IE(C_2H_4O) = 11.05 \pm 0.20 \text{ eV}$$

$$C_2H_4O^+ (\mathbf{2}) \xrightarrow{\Delta E_9} C^+ + CH_2 (\mathbf{7}) + OH + H \quad (9)$$

$$\text{or } C^+ + CH_2 (\mathbf{7}') + OH + H$$

$$\Delta E_9 = AE(C^+) - IE(C_2H_4O) = 15.32 \pm 0.30 \text{ eV}$$

In the above calculations, for $IE(C_2H_4O)$, we have used the experimental IE of ethylene oxide measured in this work. The above dissociation energies, along with those calculated by the G2 method (using the results given in Table 2), are tabulated in Table 3 for easy comparison. It is seen that the G2 and experimental dissociation energies are in excellent accord with each other. In other words, these proposed dissociation channels are supported by accurate ab initio results. Still, some uncertainties remain. For instance, for reaction 7, when $C_2H_4O^+$ dissociates to form $CH_2^+$ (**10**), the accompanying products may be formaldehyde or CO plus $H_2$. Neither experimental data nor G2 calculations can make the distinction. While the G2 results indicate that $CH_2O$ is the more likely side product, neither of the two possibilities can be ruled out. A similar situation exists in reaction 9, where either the singlet or triplet methylene is one of the products. Energetically, G2 results favor the singlet state.

**Dissociation Channels Involving Transition Structure(s).** In this section, we consider the dissociations of the ethylene oxide cation which involve one or more transition structures.

$$C_2H_4O^+ (\mathbf{2}) \xrightarrow{\Delta E_{10}} CHO^+ (\mathbf{12}) + CH_3 (\mathbf{13}) \quad (10)$$

$$\Delta E_{10} = AE(CHO^+) - IE(C_2H_4O) = 0.97 \pm 0.02 \text{ eV}$$

To yield $CHO^+$ (**12**) and $CH_3$ (**13**) from a dissociation of **2**, **2** first undergoes a hydrogen transfer and ring opening via TSa to form intermediate cation **14**. Cation **14** then undergoes bond cleavage reaction to produce $CHO^+$ and $CH_3$. The energy profile of this process is shown in Figure 8. The reaction barrier is calculated to be 0.96 eV, in good agreement with the experimental dissociation energy, 0.97 ± 0.02 eV.

**TABLE 3: Experimental and Calculated Energies (eV) of the Dissociations of the Ethylene Oxide Cation**

| dissociation reactions | $\Delta E$ (exptl) | $\Delta E$ (G2) or reaction barrier |
|---|---|---|
| Simple Bond Cleavage Reactions | | |
| (1) $C_2H_4O^+$ (**2**) → $C_2H_3O^+$ (**3**) + H | 1.29 ± 0.02 | 1.34[a] |
| (2) $C_2H_4O^+$ (**2**) → $C_2H_2O^+$ (**4**) + $H_2$ | 3.11 ± 0.03 | 3.27 |
| (3) $C_2H_4O^+$ (**2**) → $C_2HO^+$ (**5**) + $H_2$ + H | 6.95 ± 0.15 | 6.86 |
| (4) $C_2H_4O^+$ (**2**) → $CH_2O^+$ (**6**) + $CH_2$ (**7**) | 3.74 ± 0.10 | 3.72 |
| (5) $C_2H_4O^+$ (**2**) → $C_2H_4^+$ (**8**) + O | 3.67 ± 0.03 | 3.64 |
| (6) $C_2H_4O^+$ (**2**) → $C_2H^+$ (**9**) + 3H + O | 17.04 ± 0.30 | 16.94 |
| (7) $C_2H_4O^+$ (**2**) → $CH_2^+$ (**10**) + $CH_2O$ (**11**) | 3.14 ± 0.03 | 3.08 |
| or $CH_2^+$ (**10**) + CO + $H_2$ | | 2.94 |
| (8) $C_2H_4O^+$ (**2**) → $CH^+$ ($^1\Sigma$) + $CH_2$ (**7**) + OH | 11.05 ± 0.20 | 11.01 |
| (9) $C_2H_4O^+$ (**2**) → $C^+$ + $CH_2$ (**7**) + OH + H | 15.32 ± 0.30 | 15.12 |
| or $C^+$ + $CH_2$ (**7′**) + OH + H | | 15.41 |
| Reactions Involving Transition Structure(s) | | |
| (10) $C_2H_4O^+$ (**2**) → $CHO^+$ (**12**) + $CH_3$ (**13**) | 0.97 ± 0.02 | 0.96 |
| (11) $C_2H_4O^+$ (**2**) → $CH_4^+$ (**15**) + CO | 0.99 ± 0.02 | ~0.96 |
| (12) $C_2H_4O^+$ (**2**) → $C_2H_2^+$ (**17**) + $H_2O$ (**18**) | 1.30 ± 0.06 | 1.48 |
| (13) $C_2H_4O^+$ (**2**) → $C_2H_3^+$ (**21**) + OH | 2.27 ± 0.02 | 2.23 |
| (14) $C_2H_4O^+$ (**2**) → $CH_3^+$ (**23**) + CO + H | 2.79 ± 0.03 | 2.88 |
| (15) $C_2H_4O^+$ (**2**) → $CH_3O^+$ (**26**) + CH ($^4\Sigma$) | 4.61 ± 0.10 | 4.64 |

[a] A TS was located for this reaction, but its energy is very close to that of the products (see text).

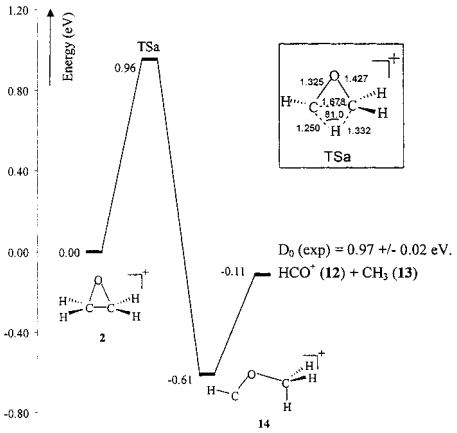


**Figure 8.** Potential energy surface showing the possible mechanism for dissociation $C_2H_4O^+ \rightarrow HCO^+ + CH_3$.

$$C_2H_4O^+ (\mathbf{2}) \xrightarrow{\Delta E_{11}} CH_4^+ (\mathbf{15}) + CO \quad (11)$$

$$\Delta E_{11} = AE(CH_4^+) - IE(C_2H_4O) = 0.99 \pm 0.02 \text{ eV}$$

The energy profile of this reaction is shown in Figure 9. As in reaction 10, cation **14** is first formed via TSa. Then **14** undergoes rotation around one of the C−O bonds to form **16** via TSb. Cation **16** has the proper arrangement to dissociate into $CH_4^+$ (**15**) and CO via a cyclic four-center transition state TSc. However, we failed to locate TSc after repeated attempts. In any event, if the energy of TSc is lower, or not much higher, than that of TSa, the reaction barrier would still be in good agreement with the experimental dissociation energy, 0.99 ± 0.02 eV.

$$C_2H_4O^+ (\mathbf{2}) \xrightarrow{\Delta E_{12}} C_2H_2^+ (\mathbf{17}) + H_2O (\mathbf{18}) \quad (12)$$

$$\Delta E_{12} = AE(C_2H_2^+) - IE(C_2H_4O) = 1.30 \pm 0.06 \text{ eV}$$

The energy profile of this reaction is given in Figure 10. In this

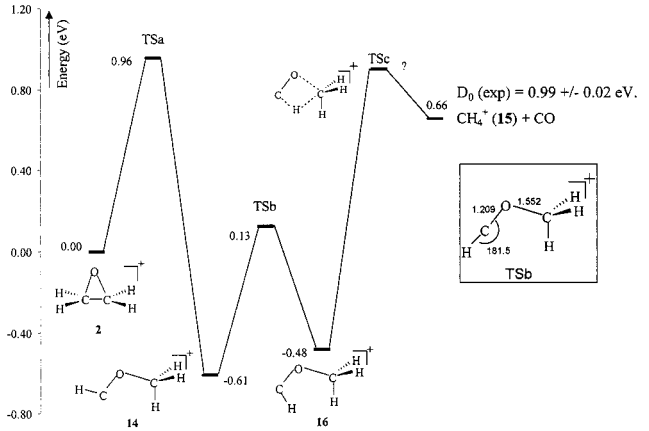


**Figure 9.** Potential energy surface showing the possible mechanism for dissociation $C_2H_4O^+ \rightarrow CH_4^+ + CO$.

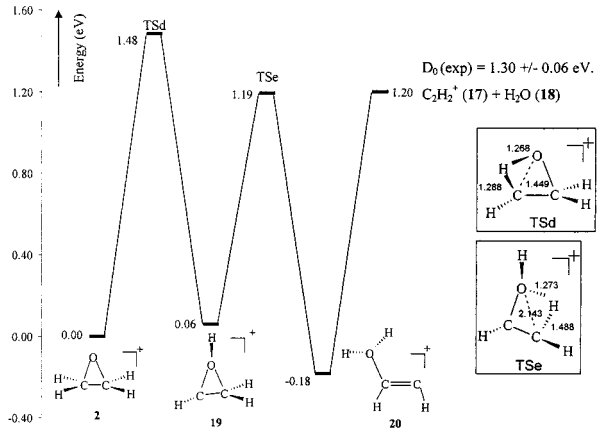


**Figure 10.** Potential energy surface showing the possible mechanism for dissociation $C_2H_4O^+ \rightarrow C_2H_2^+ + H_2O$.

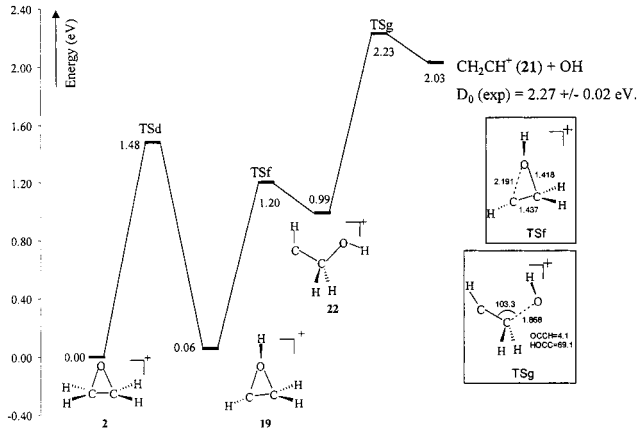


**Figure 11.** Potential energy surface showing the possible mechanism for dissociation $C_2H_4O^+ \rightarrow CH_2CH^+ + OH$.

figure, we see that **2** undergoes two hydrogen shifts via TSd, intermediate **19**, and TSe to form cation **20**, which then cleaves its C−O bond to produce ethylene cation **17** and water. The G2 barrier of this reaction is 1.48 eV, in fair agreement with the experimental dissociation energy, 1.30 ± 0.06 eV.

$$C_2H_4O^+ (\mathbf{2}) \xrightarrow{\Delta E_{13}} C_2H_3^+ (\mathbf{21}) + OH \qquad (13)$$

$$\Delta E_{13} = AE(C_2H_3^+) - IE(C_2H_4O) = 2.27 \pm 0.02 \text{ eV}$$

The energy profile of this reaction is shown in Figure 11. In this reaction, **2** undergoes hydrogen transfer to form **19** via TSd.

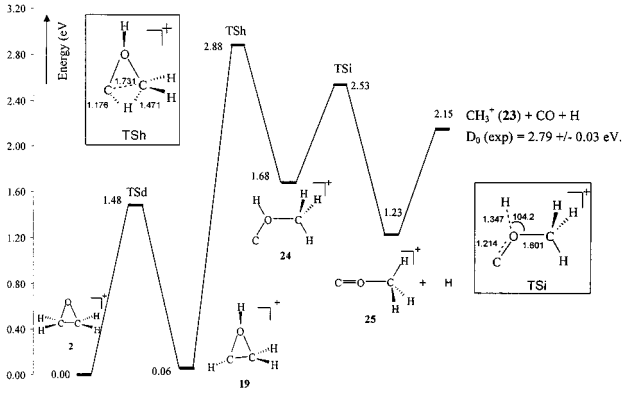


**Figure 12.** Potential energy surface showing the possible mechanism for dissociation $C_2H_4O^+ \rightarrow CH_3^+ + CO + H$.

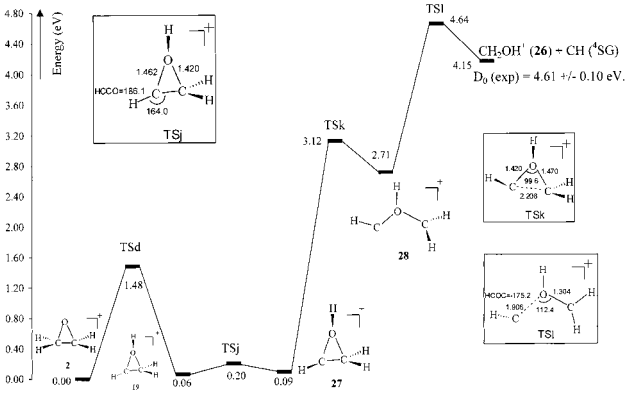


**Figure 13.** Potential energy surface showing the possible mechanism for dissociation $C_2H_4O^+ \rightarrow CH_2OH^+ + CH\ (^4\Sigma)$.

Cation **19** then undergoes ring opening by breaking one of the C−O bonds to form **22** via TSf; **22** then dissociates to $CH_2$-$CH^+$ (**21**) and OH by way of TSg. The barrier of this reaction is 2.23 eV, in excellent agreement with the experimental dissociation energy, 2.27 ± 0.02 eV.

$$C_2H_4O^+ (\mathbf{2}) \xrightarrow{\Delta E_{14}} CH_3^+ (\mathbf{23}) + CO + H \qquad (14)$$

$$\Delta E_{14} = AE(CH_3^+) - IE(C_2H_4O) = 2.79 \pm 0.03 \text{ eV}$$

The energy profile of this reaction is shown in Figure 12. As in reaction 13, **19** is first formed. Then it undergoes ring opening reaction by breaking the C−C bond and hydrogen transfer to form **24** via TSh. Cation **24** then cleaves its O−H bond via TSi to produce $CH_3OC^+$ (**25**) and H. Cation **25** undergoes bond cleavage reaction to produce $CH_3^+$ (**23**) and CO. The reaction barrier is calculated to be 2.88 eV, in fair agreement with the experimental dissociation energy, 2.79 ± 0.03 eV.

$$C_2H_4O^+ (\mathbf{2}) \xrightarrow{\Delta E_{15}} CH_3O^+ (\mathbf{26}) + CH\ (^4\Sigma) \qquad (15)$$

$$\Delta E_{15} = AE(CH_3O^+) - IE(C_2H_4O) = 4.61 \pm 0.10 \text{ eV}$$

The energy profile of this reaction is shown in Figure 13. As in the previous three reactions, **19** is first formed. Then it undergoes inversion via TSj at one of the carbons to form **27**. Afterward **27** undergoes ring opening by breaking the C−C bond to form **28** via TSk. Cation **28** then dissociates to form the products by way of TSl. The calculated barrier is 4.64 eV, in very good accord with the experimental dissociation energy, 4.61 ± 0.10 eV.

The dissociation energies and the G2 barriers for reactions (10) to (15) are included in Table 3 for easy comparison. As can be seen from these results, the agreements between theory and experiment are uniformly good.

## Conclusions

By combining the techniques of synchrotron radiation, molecular beam and mass spectrometry, we have measured the AEs of $C_2H_4O^+$, $C_2H_3O^+$, $C_2H_2O^+$, $C_2HO^+$, $CH_3O^+$, $CH_2O^+$, $CHO^+$, $C_2H_4^+$, $C_2H_3^+$, $C_2H_2^+$, $C_2H^+$, $CH_4^+$, $CH_3^+$, $CH_2^+$, $CH^+$, and $C^+$ in the dissociative photoionizations of ethylene oxide. With the aid of ab initio Gaussian-2 results, we have established the dissociation channels for the formation of these fragments.

**Acknowledgment.** W.K.L. and K.C.L. are grateful for the support of a Direct Grant from The Chinese University of Hong Kong (CUHK). They also wish to thank the Computer Services Centre at CUHK for generous allocation of computation time on the SGI Origin 2000 High Performance Server. This project (Project 29673037) is partially supported by the National Natural Science Foundation of China.

## References and Notes

(1) Hua, W. *Heterocyclic Chemistry*; Peking University Press: Beijing, 1991 (in Chinese).
(2) Gallegos, E. J.; Kiser, R. W. *J. Am. Chem. Soc.* **1961**, *83*, 773.
(3) Krassig, R.; Reinke, D.; Baumgartel, H. *Ber. Bunsen-Ges. Phys. Chem.* **1974**, *78*, 425.
(4) Holmes, J. L.; Terlouw, J. K.; Lossing, F. T. *J. Phys. Chem.* **1976**, *80*, 2860. Burgers, P. C.; Holmes, J. L. *Org. Mass. Spectrom.* **1982**, *17*, 123.
(5) Holmes, J. L.; Lossing, F. P. *Org. Mass Spectrom.* **1991**, *26*, 537.
(6) Basch, H.; Robin, M. B.; Kuebler, N. A.; Baker, C.; Turner, D. W. J. *Chem. Phys.* **1969**, *51*, 52.
(7) Aue, D. H.; Webb, H. M.; Bowers, M. T. *J. Am. Chem. Soc.* **1975**, *97*, 4137.
(8) Corderman, R. P.; LeBreton, P. R.; Buttrill, S. E., Jr.; Williamson, A. D.; Beauchamp, J. L. *J. Chem. Phys.* **1976**, *65*, 4929.
(9) Aue, D. H.; Webb, H. M.; Davidson, W. R. *J. Am. Chem. Soc.* **1980**, *102*, 5151.
(10) Beiri, G.; Asbrink, L.; Niessen, W. *J. Electron. Spectrosc. Relat. Phenom.* **1982**, *27*, 129.
(11) Watanabe, K. *J. Chem. Phys.* **1957**, *26*, 542.
(12) Johnson, K.; Powis, I.; Danby, C. J. *Chem. Phys.* **1982**, *70*, 329.
(13) Qi, F.; Sheng, L.; Zhang, Y.; Yu, S.; Li, W.-K. *Chem. Phys. Lett.* **1995**, *234*, 450.
(14) Sheng, L.; Qi, F.; Tao, L.; Zhang, Y.; Yu, S.; Wong, C.-K.; Li. W.-K. *Int. J. Mass. Spectrom. Ion Processes* **1995**, *148*, 179.
(15) Sheng, L.; Qi, F.; Gao, H.; Zhang, Y.; Yu, S.; Li, W.-K. *Int. J. Mass Spectrom. Ion Processes* **1997**, *161*, 151.
(16) Li, Q.; Ran, Q.; Chen, C.; Yu, S.; Ma, X.; Sheng, L.; Zhang, Y.; Li, W.-K. *Int. J. Mass Spectrom. Ion Processes* **1996**, *153*, 29.
(17) Curtiss, L. A.; Raghavachari, K.; Trucks, G. W.; Pople, J. A. *J. Chem. Phys.* **1991**, *94*, 7221.
(18) Frisch, M. J.; Trucks, G. W.; Schlegel, H. B.; Gill, P. M. W.; Johnson, B. J.; Robb, M. A.; Cheeseman, J. R.; Keith, T. A.; Petersson, G. A.; Montgomery, J. A.; Raghavachari, K.; Al-Laham, M. A.; Zarkrewski, V. G.; Ortiz, J. V.; Foresman, J. B.; Cioslowski, J.; Stefanov, B. B.; Nanayakkara, A.; Challacombe, M.; Peng, C. Y.; Ayala, P. Y.; Chen, W.; Wong, M. W.; Andres, J. L.; Replogle, E. S.; Gomperts, R.; Martin, R. L.; Fox, D. J.; Binkley, J. S.; Defrees, D. J.; Baker, J.; Stewart, J. J. P.; Head-Gordon, M.; Gonzalez, C.; Pople, J. A. *GAUSSIAN 94*, Revision D4; Gaussian, Inc.: Pittsburgh, PA, 1995.
(19) Traeger, J. C.; Kompe, B. W. *Int. J. Mass Spectrom. Ion Processes* **1990**, *101*, 111.
(20) Tsai, B. P.; Baer, T.; Werner, A. S.; Lin, S. F. *J. Chem. Phys.* **1975**, *79*, 570.
(21) Shiromaru, H.; Achiba, Y.; Kimura, K.; Lee, Y. T. *J. Phys. Chem.* **1987**, *91*, 17.
(22) Norwood, K.; Ali, A.; Flesch, G. D.; Ng, C. Y. *J. Am. Chem. Soc.* **1990**, *112*, 7502.